Pergamon

Int. J. Heat Mass Transfer. Vol. 38, No. 11, pp. 1923–1932, 1995

0017-9310/95 $9.50 + 0.00

0017-9310(94)00321-1

Analysis of the heat transfer coefficient in a turbulent particle pipe flow

R. AVILA†§ and J. CERVANTES‡

†Instituto Nacional de Investigaciones Nucleares, Sierra Mojada 447, Lomas de Barrilaco, D.F. 11010, México

‡Facultad de Ingeniería, Universidad Nacional Autónoma de México, D.F. 04510, México

(*Received* 17 *May* 1993 *and in revised form* 22 *October* 1994)

Abstract—A Eulerian–Lagrangian mathematical model is used to predict the average heat transfer coefficient at the inner wall of a vertical pipe. Air flows within the pipe in a turbulent regime loaded with spherical glass particles of uniform size 70, 140 and 200 μm in diameter. The suspension flow is predicted by solving numerically the mass, momentum and energy equations for the continuous phase and the motion and energy equations for individual particles. The turbulence of the air flow is calculated by using a standard $K-\varepsilon$ model and the dispersion of the particles is predicted by the Lagrangian stochastic deterministic model. The average heat transfer coefficient of the suspension is calculated for different Reynolds numbers, particle loading ratios and particle diameters. The results are compared with experimental data published in the literature.

1. INTRODUCTION

Turbulent particle flows are characterized by the simultaneous presence of a continuous gas (or liquid) phase and a dispersed particle phase with an exchange of mass, momentum and energy between both phases. The extent of these interactions depends on many factors, among them the size, concentration and physical properties of the particles and the velocity, temperature and turbulent intensity of the flow. The evaluation of the parameters that characterize these interactions gives rise to a better understanding of the physical phenomena involved.

Research in the area of heat, mass and momentum transfer in particulate flows has grown steadily in the engineering disciplines due to the increasing need to understand, evaluate and control in an optimal way the interaction between the two phases. With an appropriate knowledge of the parameters that control the interchange mechanisms between the phases it will be possible to increase the efficiency of the gasification and combustion of pulverized coal and atomized liquid fuels, to decrease the erosion of pipes and turbines, and control the dispersion of the contaminants in the atmosphere, rivers and seas, etc.

One of the phenomena that have been studied from the experimental, analytical and numerical point of view [1–16] that is still not properly understood is the heat transfer between the wall of a duct and a turbulent flow transporting either solid or liquid particles. In these flows, the interaction mechanisms between the phases are a complex function of several factors (mean velocity, turbulence intensity, thermophysical properties, particle size, particle loading ratio, etc.), and give rise to a particular behavior of both the local (wall-suspension) and the average heat transfer.

In the literature it is reported (see the surveys in refs. [1–3]) that some authors have measured or predicted an increase of the heat transfer through the wall when small solid particles are added to the flow [4, 6–10, 15], whereas other researchers have detected that, as the particle loading ratio increases, the heat transfer first decreases to a minimum value and then (depending on the suspension characteristics), it can increase, remain without significant change, or even decrease [5, 11–14, 16].

Depew and Kramer [3] present a discussion of the different parameters that affect the rate of heat transfer from the wall to the suspension. They pointed out that the heat transfer is affected by the addition of particles which modify the turbulent structure of the flow and promote the exchange of energy between the viscous sublayer and the turbulent core.

In this paper, an analysis of the heat transfer from a vertical pipe with constant wall temperature to a turbulent particle flow is presented. The purpose of the work is to identify the influence that small spherical solid particles have on the suspension average heat transfer coefficient, as the Reynolds number, particle diameter and particle loading ratio are changed. The experiment of Farbar and Depew [4], is reproduced satisfactorily, and it is verified by the simulation of the Tsuji *et al.* experiment [17], that both the turbulence intensity of pipe flow decreases at low particle loading ratio ($0 < ZL < 1$) and that turbulence is promoted

§To whom correspondence should be addressed.

NOMENCLATURE

A_p particle surface area [m^2]
A_{transf} heat transfer surface area [m^2]
Bi Biot number
c_p fluid specific heat [J kg^{-1} K^{-1}]
C_p particle specific heat [J kg^{-1} K^{-1}]
D pipe diameter [m]
d_p particle diameter [m]
g acceleration of gravity [m s^{-2}]
H mean fluid total enthalpy [m^2 s^{-2}]
$\bar{h}$ average heat transfer coefficient [W m^{-2} K^{-1}]
k thermal conductivity of the fluid [W m^{-1} K^{-1}]
K turbulent kinetic energy [m^2 s^{-2}]
L pipe length [m]
m_f mass flow rate of the gas [kg s^{-1}]
m_p mass flow rate of the solid phase [kg s^{-1}]
n_p number of particles within a control volume
$\dot{N}_j^p$ number of particles per unit of time in the jth trajectory [1 s^{-1}]
$\overline{Nu}$ average Nusselt number
Pe Peclet number
Pr Prandtl number
p pressure [N m^{-2}]
Q heat flow [W]
r_o pipe radius [m]
r_p particle position in the radial direction [m]
r radial direction [m]
Re Reynolds number
$\bar{T}$ mean fluid temperature [K]
T instantaneous temperature [K]
T_{buli}, T_{bulo} suspension bulk temperature at the inlet and outlet of the heated section
T_{mfi}, T_{mfo} gas phase bulk temperature at the inlet and outlet of the heated section
T_{mpi}, T_{mpo} solid phase bulk temperature at the inlet and outlet of the heated section
t time [s]
U_f mean velocity of the gas phase [m s^{-1}]
V_p particle volume [m^3]
ZL loading ratio, mass flow rate of solids over mass flow rate of air.

Greek symbols
Δt time interval [s]
ΔV fluid volume [m^3]
ΔTlm logarithmic mean temperature difference [K]
ε dissipation rate of K [m^2 s^{-3}]
θ angular direction
μ dynamic viscosity [kg m^{-1} s^{-1}]
ν kinematic viscosity [m^2 s^{-1}]
ρ fluid density [kg m^{-3}]
ρ_p particle density [kg m^{-3}]
τ_p dynamic characteristic time of the particle [s]
τ_{pter} thermal characteristic time of the particle [s]
ϕ general variable.

Subscripts
E Eulerian
L Lagrangian
p refers to the particles
po initial value prior Δt
s refers to the surface of the pipe
susp refers to the suspension
t refers to turbulent flow.

when the loading is of the order of greater than one. This explains the phenomenon that many authors have observed either experimentally or numerically concerning the variation of the average heat transfer coefficient at loading ratios around one.

The numerical computations carried out in this work verify that, at a loading ratio larger than one, the increase in the heat capacity of the suspension is the primary factor that promotes the increase in the average heat transfer coefficient.

The mean values of velocity and temperature of the gas phase are obtained by solving the mass, momentum and energy conservation equations together with a standard ($K-\varepsilon$) turbulence model. The velocity and temperature histories of isolated particles are found by solving their momentum and energy Lagrangian equations.

The dispersion of the particles in the turbulent flow is determined using the LSD (Lagrangian-stochastic-deterministic) model [18], which requires the values of the instantaneous gas phase flow velocities and temperatures.

The instantaneous flow properties of the continuous phase are determined through the generation of Gaussian random numbers. The mean and turbulent characteristics of the dispersed phase are obtained by averaging a statistically significant number of trajectories.

As the suspension flow was very dilute, no consideration was given to heat and momentum exchange between the particles. The temperatures in the system were assumed to be small, so that the radiation heat transfer between the pipe and the mixture was neglected. As mentioned before, the walls of the vertical pipe

Table 1. ϕ, μ_{eff}/Pr_{eff} and S_ϕ expressions for the transport equations of the gas

ϕ	$\frac{\mu_{eff}}{Pr_{eff}}$	S_ϕ
$\bar{u}$	$\mu+\mu_t$	$-\frac{dp}{dx}+\rho g$
H	$\frac{\mu}{Pr}+\frac{\mu_t}{Pr_t}$	$\frac{1}{r}\frac{\partial}{\partial r}\left(r\left(\mu_{eff}\left(1-\frac{1}{Pr_{eff}}\right)\frac{1}{2}\frac{\partial \overline{u^2}}{\partial r}\right)\right)+\rho\bar{u}g$
K	$\frac{\mu_t}{\sigma_K}$	$\mu_t\left(\frac{\partial \bar{u}}{\partial r}\right)^2-\rho\varepsilon$
ε	$\frac{\mu_t}{\sigma_\varepsilon}$	$C_1\mu_t\frac{\varepsilon}{K}\left(\frac{\partial \bar{u}}{\partial r}\right)^2-C_2\rho\frac{\varepsilon^2}{K}$

are assumed to be at a constant temperature and the average heat transfer coefficient is calculated by defining a logarithmic mean temperature difference.

2. MATHEMATICAL FORMULATION (CONTINUOUS PHASE)

The mean values of velocity, temperature and turbulent quantities of the gas phase are obtained by solving the transport equations of mass, momentum and energy, together with the standard $K-\varepsilon$ turbulence model [19], which requires the formulation of one equation for the turbulence kinetic energy (K) and another one for its dissipation rate (ε).

The system of differential parabolic equations in cylindrical coordinates can be formulated as one general equation:

$$\rho\bar{u}\frac{\partial\phi}{\partial x}+\rho\bar{v}\frac{\partial\phi}{\partial r}=\frac{1}{r}\frac{\partial}{\partial r}\left(r\frac{\mu_{eff}}{Pr_{eff}}\frac{\partial\phi}{\partial r}\right)+S_\phi+S_\phi^P. \quad (1)$$

The variables ϕ, (μ_{eff}/Pr_{eff}) and S_ϕ, have a different form, depending on the transport equation considered. The expressions for these variables are presented in Table 1.

The interaction source terms $S_{\bar{u}}^P, S_H^P, S_K^P$ and S_ε^P of equation (1) represent the exchange of momentum, total enthalpy, turbulence kinetic energy and dissipation rate between the phases, respectively.

The values of the constants that appear in the turbulence model are shown in Table 2 [19].

3. MATHEMATICAL FORMULATION (PARTICULATE PHASE)

3.1. *Particle momentum equation*

The Lagrangian momentum equation of an individual spherical particle in a gas stream is a complicated function of different phenomena which appear in the near vicinity of the particle. In order to establish the Lagrangian momentum equation, the particle is assumed to be isolated and far from any boundary so that particle–particle interactions, and particle–boundary interactions are not considered. The contribution of the mean pressure gradients of the gas phase to the force on the particles, the particle thermal (Brownian) motion, the effect of neighboring particles on drag forces and the variations in particle size and shape are all neglected [20]. Virtual mass and Basset terms are not included in the equation because they are of the order of the gas–particle density ratio [21], which for the calculations performed in this research is 10^{-3}. The Saffman lift and Magnus forces are neglected because the particles are not in a high shear gas phase flow. It is assumed that the particle size is much lower than the characteristic length of the flow, where changes of the mean flow properties are supposed to occur [22]. It is assumed that the only body force acting on the particles is the gravity force. Finally drag is treated empirically, assuming quasi-steady flow for spherical particles [23].

Table 2. Constants for the $K-\varepsilon$ turbulence model

C_μ	C_1	C_2	σ_K	σ_ε
0.09	1.44	1.92	1.0	1.3

With the assumptions mentioned before, the Lagrangian equations that describe the movement of the particles in the polar–cylindrical coordinate system are [24]

$$\frac{du_p}{dt}=\frac{(u-u_p)}{\tau_p}+g\left(1-\frac{\rho}{\rho_p}\right) \quad (2)$$

$$\frac{dv_p}{dt}=\frac{(v-v_p)}{\tau_p}+\frac{w_p^2}{r_p} \quad (3)$$

$$\frac{dw_p}{dt}=\frac{(w-w_p)}{\tau_p}-\frac{w_p v_p}{r_p} \quad (4)$$

where

$$w_p=r_p\frac{\partial\theta}{\partial t}$$

$$\tau_p=\frac{m_p}{3\pi\mu f d_p}$$

$$f=1+0.15Re_p^{0.687}$$

$$Re_p=\frac{\rho d_p U}{\mu}$$

$$U=((u-u_p)^2+(v-v_p)^2+(w-w_p)^2)^{1/2}.$$

The trajectory of individual particles is known when the momentum equations (2)–(4) are integrated along the flow domain, the integration is performed by using small time intervals and assuming that the forces acting on the particles remain constant during each interval.

The momentum equations (3)–(4), are solved numerically by using a second order Runge–Kutta algorithm. The resulting explicit expressions are:

axial direction,

$$u_p = u-(u-u_{po})\exp\left(-\frac{\Delta t}{\tau_p}\right) -g\left(1-\frac{\rho}{\rho_p}\right)\left(1-\exp\left(-\frac{\Delta t}{\tau_p}\right)\right)\tau_p \quad (5)$$

radial direction,

$$v_p = v_{po}+\frac{\Delta t}{2}\left(-\frac{v_{po}}{\tau_p}+\frac{w_{po}^2}{r_{po}}-\frac{\overline{V_p}}{\tau_p}+\frac{\overline{W_p^2}}{r_{po}}+2v\right) \quad (6)$$

angular direction,

$$w_p = w_{po}+\frac{\Delta t}{2}\left(-\frac{w_{po}}{\tau_p}-\frac{w_{po}v_{po}}{r_{po}} -\frac{\overline{W_p}}{\tau_p}-\frac{\overline{W_p}\,\overline{V_p}}{r_{po}}+2w\right) \quad (7)$$

where

$$\overline{V_p} = v_{po}+\Delta t\left(-\frac{v_{po}}{\tau_p}+\frac{w_{po}^2}{r_{po}}\right)$$

$$\overline{W_p} = w_{po}+\Delta t\left(-\frac{w_{po}}{\tau_p}-\frac{w_{po}v_{po}}{r_{po}}\right).$$

The location of individual particles is calculated by the following expressions:

$$x_p = x_{po}+\frac{\Delta t}{2}(u_p+u_{po}) \quad (8)$$

$$r_p = r_{po}+\frac{\Delta t}{2}(v_p+v_{po}) \quad (9)$$

$$\theta_p = \theta_{po}+\frac{\Delta t}{2}\left(\frac{w_p}{r_p}+\frac{w_{po}}{r_{po}}\right). \quad (10)$$

In the solution of the particle momentum equations it is assumed that the particles do not lose kinetic energy when they impact the wall of the duct (elastic reflection). Consequently, the particles leave the wall at the same angle and velocity as they approach it.

3.2. *Particle heat balance equation*

In this work, it is assumed that the particles do not receive heat directly from the wall when they impact it, i.e. the heat is transmitted first from the wall to the fluid and then to the particles.

The heat balance equation of an isolated particle in a gas stream is formulated using the following assumptions:

The particles do not undergo phase change or chemical reaction.

The temperature gradients in the particle are negligible (small particle Biot number).

The radiation heat transfer between the wall and the flow is neglected (wall-flow system at low temperature).

The particle heat balance equation is formulated as:

$$Q = \rho_p V_p C_p \frac{dT_p}{dt} \quad (11)$$

where

$$Q = -\bar{h}A_p(T_p-T) \quad (12)$$

$$\bar{h} = \frac{\overline{Nu}\,k}{d_p}. \quad (13)$$

The average particle Nusselt number is a function of both the particle Reynolds number and the fluid Prandtl number. Three empirical correlations are used to calculate the average particle Nusselt number [25].

(A) $0 \leqslant Re_p \leqslant 1$

$$\overline{Nu} = 1+(1+Pe)^{0.333}$$

(B) $1 \leqslant Re_p \leqslant 100$

$$\overline{Nu} = Re_p^{0.41}\left(1+\frac{1}{Pe}\right)^{0.333}Pr^{0.333}+1$$

(C) $100 \leqslant Re_p \leqslant 2000$

$$\overline{Nu} = 0.752Re_p^{0.472}\left(1+\frac{1}{Pe}\right)^{0.333}Pr^{0.333}+1.$$

The integration of the heat equation (11) is performed using a small time interval Δt and assuming that the instantaneous fluid temperature remains constant during this interval. The instantaneous particle temperature is then

$$T_p = (T_{po}-T)\exp\left(-\frac{\Delta t}{\tau_{pter}}\right)+T \quad (14)$$

where

$$\tau_{pter} = \frac{\rho_p d_p^2 C_p}{6\overline{Nu}\,k}. \quad (15)$$

The energy transfer (particle–fluid) during Δt is:

$$E = \frac{\rho_p \pi d_p^3 C_p(T_{po}-T)}{6}\left(1-\exp\left(-\frac{\Delta t}{\tau_{pter}}\right)\right). \quad (16)$$

The calculation of a relatively high number of particle trajectories (2000) allows the evaluation of both the mean characteristics of the dispersed phase and the interaction source terms.

4. PARTICLE DISPERSION MODEL

Particle dispersion by fluid turbulent eddies is predicted by use of the LSD model developed by Milojevic [18]. The LSD model requires the knowledge of the mean Eulerian characteristics (velocity, temperature, K and ε) of the continuous phase in order to calculate the Lagrangian length and time scales of the turbulent eddies, which promote particle dispersion.

The life time of the Lagrangian eddies is calculated as

$$t_L = 0.3\frac{K}{\varepsilon}. \tag{17}$$

The length of the Lagrangian eddies is calculated by the following expression

$$L_L = urms\, t_L. \tag{18}$$

In the last equation it is assumed that the turbulence of the gas phase is isotropic, homogeneous and steady [26], i.e.

$$(urms)_L = (urms)_E = urms \tag{19}$$

where

$$urms = (\tfrac{2}{3}K)^{1/2}. \tag{20}$$

The velocity and temperature fluctuations of the continuous phase, are generated as random numbers with a Gaussian probability distribution with standard deviations *urms* and *Trms*, respectively. A *Trms* expression developed by Launder [27], is used in the following form:

$$(\overline{T'^2})^{1/2} = Trms = \left(-\frac{2RK\mu_t}{\varepsilon\rho Pr_t}\left(\frac{\partial\bar{T}}{\partial r}\right)^2\right)^{1/2} \tag{21}$$

where

$$R = \frac{\text{thermal eddy life time}}{\text{dynamic eddy life time}}.$$

As a first approximation, the life times of the thermal and dynamic eddies are assumed to be the same i.e. $R = 1$.

The instantaneous values of velocity and temperature of the gas phase are calculated as:

$$u = \bar{u} + u' \tag{22}$$

$$T = \bar{T} + T'. \tag{23}$$

The generated fluctuations remain constant during the particle–eddy interaction time;

$$t_{intera} = \min(t_L, t_{transit}) \tag{24}$$

where

$$t_{transit} = \frac{L_L}{v_{rel}} \tag{25}$$

$$v_{rel} = \max(|u-u_p|, |v-v_p|, |w-w_p|). \tag{26}$$

The LSD model [18] assumes that a new fluctuation must be generated when any of the following situations occur: the particle crosses the eddy; the eddy life time is over.

5. MEAN CHARACTERISTICS OF THE DISPERSED PHASE AND SOURCE TERMS

In order to calculate both the mean characteristics (velocity, temperature, concentration and turbulent kinetic energy) of the particles, and the interaction term S_ϕ^p, a relatively high number of particle trajectories are computed and ensembles averaged.

The equations that the LSD model requires to calculate the mean dynamic characteristics of the disperse phase and the source terms (S_u^p, S_k^p and S_ε^p) are formulated by Milojevic [18]. In this section, the expressions for both the mean temperature of the particles within a Eulerian numerical control volume and the interaction term S_H^p will be presented.

The mean temperature of the dispersed phase in a control volume is evaluated as:

$$\overline{T_p} = \frac{1}{n_p}\sum_j\sum_{t_1}^{t_2} T_p \dot{N}_j^p \Delta t \tag{27}$$

where

$$n_p = \sum_j\sum_{t_1}^{t_2} \dot{N}_j^p \Delta t. \tag{28}$$

$(t_2-t_1) \equiv$ time that the particles in the jth trajectory remain in the control volume.

$\Delta t \equiv$ integration time interval.

The source term for the energy conservation equation in a control volume is:

$$S_H^p = \frac{1}{\Delta V}\sum_j\sum_{t_1}^{t_2} \rho_p V_p C_p (T_p - T) \times\left(1-\exp\left(-\frac{t}{\tau_{pter}}\right)\right)\frac{1}{\Delta t}\dot{N}_j^p \Delta t \tag{29}$$

where $\Delta V \equiv$ fluid volume in the numerical control volume.

6. NUMERICAL PROCEDURE

The general conservation equation of the gas phase equation (1), is solved numerically using the control volume algorithm developed by Patankar and Spalding [28], and explained in detail by Patankar [29]. This numerical method is the base of several computer programs which solve the parabolic equations for single phase turbulent flows [30, 31].

The numerical procedure is implicit and uses a marching technique, i.e. at any one axial location, the mean characteristics of the gas phase are required in order to evaluate the flow characteristics at the next axial location. This allows the use of a much finer grid in both the streamwise and the cross-stream directions. With this numerical information it is possible to obtain grid independent solutions and accurately compare numerical predictions with experimental results.

The numerical procedure at a given axial location x is as follows:

solve the gas phase conservation equations without particles, from x to $x+\Delta x$ (next axial position);

start particle trajectories from x to $x+\Delta x$ (evaluate particle position and temperature history);

evaluate the mean characteristics of the particles and the interaction source terms;

solve the gas phase conservation equations considering the particle source terms, from x to $x+\Delta x$;

iterate until a convergence criterion is satisfied;

solve the gas phase conservation equations without particles, from $x+\Delta x$ to $x+2\Delta x$.

The experimental works of Tsuji *et al.* [17] and Farbar and Depew [4] were predicted by using a numerical grid of 40 nodes in the radial direction and 2500 integration steps in the axial direction. The mean characteristics of the particulate phase were obtained by an ensemble average of 2000 particle trajectories.

The time increment (Δt), used in the solution of the particle equations, was adjusted in the numerical procedure, in order to have at least five integration steps for each particle trajectory in a Δx increment.

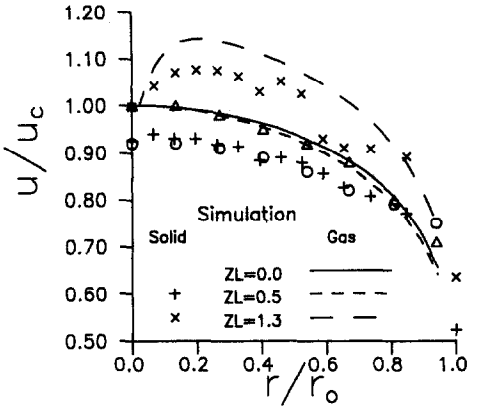

Fig. 1. Mean velocity distribution of the gas phase and solid phase for various loading ratios (Tsuji *et al.* experiment, $d_p = 200 \times 10^{-6}$ m, $Re_D = 2.1 \times 10^4$, $ZL = 1.3$, △ gas phase, ○ solid phase).

7. RESULTS AND DISCUSSION

It has been reported in the literature [1–16], that the averaged heat transfer coefficient $\bar{h}_{susp}$ (between the wall of a vertical pipe and a particulate turbulent flow) increases or decreases depending on multiple thermal and dynamic flow parameters. Most of the theoretical and experimental works, however, conclude that the variable behavior of $\bar{h}_{susp}$ is mainly the result of the following phenomena:

(a) The local convective heat transfer coefficient increases or decreases.

(b) The heat capacity of the suspension increases.

Although these phenomena have been identified, the complicated nature of $\bar{h}_{susp}$ reported in the literature allows one to conclude that the heat transfer mechanism in these flows has not been well understood [5].

In this section the numerical predictions of the experimental work of Farbar and Depew [4] are presented. Farbar and Depew characterized the averaged heat transfer coefficient $\bar{h}_{susp}$, with the following parameters varying:

particle diameter d_p;
loading ratio ZL;
suspension Reynolds number

$$Re_D = \frac{DU_f}{\nu}$$

where $D \equiv$ pipe diameter, $U_f \equiv$ mean velocity of the gas phase.

In the experiment, the wall temperature of the vertical pipe was constant. Farbar and Depew presented their paper graphs of ZL vs $\bar{h}_{susp}$, and completed only a qualitative analysis of the influence of the gas phase turbulence intensity on the average heat transfer coefficient. A quantitative analysis of this influence is presented by predicting the well characterized isothermal experiment of Tsuji *et al.* [17]. This was performed following Depew and Kramer [3] which pointed out that advances in understanding a thermal system must be based on progress in the description of an isothermal system. Tsuji *et al.* [17] measured in a vertical pipe flow the mean velocity of both phases and the turbulence intensity of the gas phase. The pipe diameter was 0.03 m and the test section was located 5 m downstream from the particle injection. Tsuji *et al.* [17] used five different kinds of particles, but in each test run the particles were of homogeneous shape, size and material. The predictions of this experiment with 200 and 500 μm polyestyrene spherical particles ($\rho = 1020$ kg m^{-3}) are presented in Figs. 1–5. In these figures the ordinate axis represents the symmetry axis of the pipe, whereas u_c is the velocity of the gas phase on that axis.

Figure 1 shows the radial distributions of the longitudinal mean velocities for both phases, with $d_p = 200$ μm, $Re_D = 2.1 \times 10^4$ and three loading ratios (0.0, 0.5, 1.3).

The radial distributions of the mean velocities for both phases, for 500 μm particles, $Re_D = 2.1 \times 10^4$ and

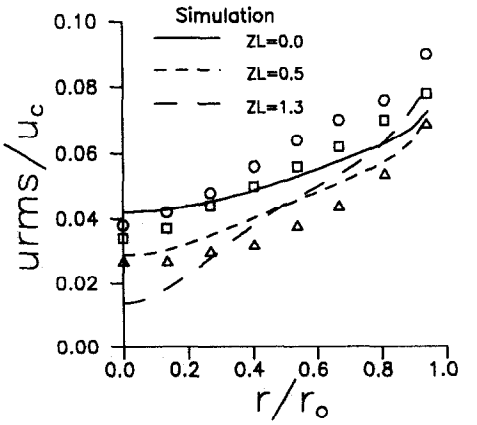

Fig. 2. *urms* distribution of the gas phase, for various loading ratios (Tsuji *et al.* experiment, $d_p = 200 \times 10^{-6}$ m, $Re_D = 2.1 \times 10^4$, ○ $ZL = 0.0$, □ $ZL = 0.5$, △ $ZL = 1.3$).

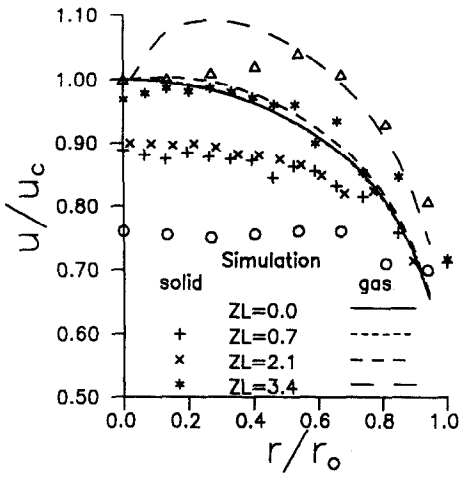

Fig. 3. Mean velocity distribution of the gas phase and solid phase for various loading ratios (Tsuji *et al.* experiment, $d_p = 500 \times 10^{-6}$ m, $Re_D = 2.1 \times 10^4$, $ZL = 3.4$, △ gas phase, ○ solid phase).

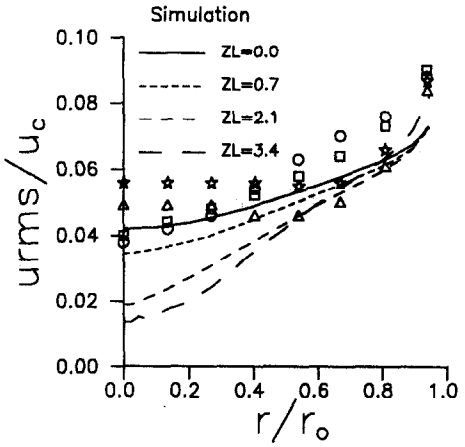

Fig. 4. *urms* distribution of the gas phase, for various loading ratios (Tsuji *et al.* experiment, $d_p = 500 \times 10^{-6}$ m, $Re_D = 2.1 \times 10^4$, ○ $ZL = 0.0$, □ $ZL = 0.7$, △ $ZL = 2.1$, ☆ $ZL = 3.4$).

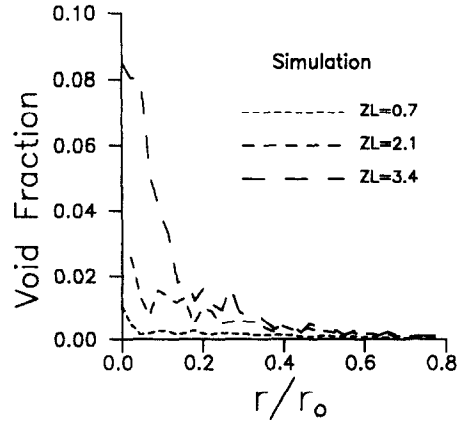

Fig. 5. Void fraction distribution, for various loading ratios (Tsuji *et al.* experiment, $d_p = 500 \times 10^{-6}$ m, $Re_D = 2.1 \times 10^4$).

four loading ratios (0.0, 0.7, 2.1, 3.4) are shown in Fig. 3.

In Figs. 1 and 3, it can be observed that the point of maximum gas phase velocity deviates from the pipe axis as the loading ratio increases, i.e. the velocity profile becomes concave, especially when the loading ratio is 1.3 ($d_p = 200$ μm) and 3.4 ($d_p = 500$ μm). Such a concave profile was reported by Tsuji *et al.* [17]. Figure 1 shows that the maximum velocity of the gas phase (ocurring out of the symmetry axis) is over-predicted when $d_p = 200$ μm and $ZL = 1.3$. However, the comparison between predicted and measured gas phase velocity in the case of 500 μm and $ZL = 3.4$ is encouraging, because both profiles show a similar trend (see Fig. 3).

Figures 2 and 4 show how the particles alter the turbulence intensity of the gas phase. It is found that the numerical calculations predict a decrease of the turbulence intensity when the loading ratio increases, a similar trend was reported by Tsuji *et al.* [17], when the flow was loaded with 200 μm particles and the loading ratio was $0 < ZL < 1.3$ (see Fig. 2).

Figure 4 shows that the calculations systematically predict a decrease of the turbulence in the region $0 < r/r_0 < 0.5$ when the loading ratio is $0 < ZL < 3.4$, however in the region $0.5 < r/r_0 < 1.0$, the predictions show a strange behavior of the turbulence intensity, especially when $ZL > 1$. It is important to observe in this figure that when $ZL > 1$ in the logarithmic region (near the wall), both the predicted values and the experimental data of the turbulence intensity are greater than those of the clean gas.

The predicted mean velocity of the particulate phase is also shown in Figs. 1 and 3. It is observed that the velocity of the 500 μm particles is almost uniform along the cross section, whereas the velocity distribution of the 200 μm particles is similar (in shape) to the velocity of the gas phase. It is observed that the velocity of the particles increases with the loading ratio and that the velocity of the particles is lower than the gas velocity in almost all the cross sections. Close to the wall, however, the particles have higher velocity. Figures 1 and 3 show that in vertical flow, particles with higher characteristic time have higher velocity.

Figure 5 shows the radial void fraction distribution for 500 μm particles. It is found that the particles concentrate around the center of the pipe, Tsuji *et al.* [17] do not report the void fraction distribution, however it is in agreement with the analytical expression developed by Kramer and Depew [32]. In the same figure it is observed that, at low loadings ($ZL = 0.7$), the void fraction distribution is almost uniform. The same behavior was found in the experimental work by Kramer [3].

The numerical predictions of Tsuji *et al.*'s experiment showed how the particles modify both the mean velocity and the turbulence intensity of the gas phase (Figs. 1–5). These results are used together with the predictions of the Farbar and Depew experiment [4] to

understand the behavior of the average heat transfer coefficient.

In nonisothermal particulate flows the local convective heat transfer coefficient depends on the thickness of the viscous sublayer, which is a function of the loading ratio and particle size.

In the literature it has been mentioned (without verification), that at low loading ratios the following phenomena appear: turbulence is suppressed, the viscous sublayer thickness increases and the local convective heat transfer coefficient decreases. On the other hand, it has been found that at high loading ratios, the particles promote turbulence, decrease the viscous sublayer thickness and increase the local heat transfer. Figures 2 and 4 verify this behavior, i.e. low loading ratio decreases the turbulence level, whereas high loading increases the turbulence intensity.

The numerical computation of Farbar and Depew experiment [4] assumes that the thermophysical properties of the gas phase are constant and that the radiation heat transfer is neglegible. It is also assumed that the temperature gradient in the particles is negligible, i.e. $Bi < 0.1$ [33].

The average heat transfer coefficient, $\bar{h}_{susp}$, is a function of both the heat transported by the suspension Q_{susp} and the logarithmic mean temperature difference ΔTlm_{susp}, i.e.

$$Q_{susp} = \bar{h}_{susp} A_{transf} \Delta Tlm_{susp} \tag{30}$$

where

$$\Delta Tlm_{susp} = \frac{\Delta T_{bulo} - \Delta T_{buli}}{\ln\left(\frac{\Delta T_{bulo}}{\Delta T_{buli}}\right)} \tag{31}$$

$$\Delta T_{buli} = T_s - T_{buli}$$

$$\Delta T_{bulo} = T_s - T_{bulo}.$$

The heat transported by the suspension is evaluated by the following relationship:

$$Q_{susp} = (m_f c_p + m_p C_p)(T_{bulo} - T_{buli}) \tag{32}$$

where

$$T_{buli} = \frac{m_f c_p T_{mfi} + m_p C_p T_{mpi}}{m_f c_p + m_p C_p} \tag{33}$$

$$T_{bulo} = \frac{m_f c_p T_{mfo} + m_p C_p T_{mpo}}{m_f c_p + m_p C_p}. \tag{34}$$

The geometrical characteristics and thermal properties that were used to predict the Farbar and Depew experiment are as follows:

Solid glass spherical particles.
Particle density 2570 kg m^{-3}.
Particle specific heat 799.63 J (kg K)$^{-1}$.
Air density 1.079 kg m^{-3}.
Air specific heat 1,008 J (kg K)$^{-1}$.
Pipe length 0.806 m.
Pipe diameter 0.017 m.
Heat transfer surface 0.043 m^2.

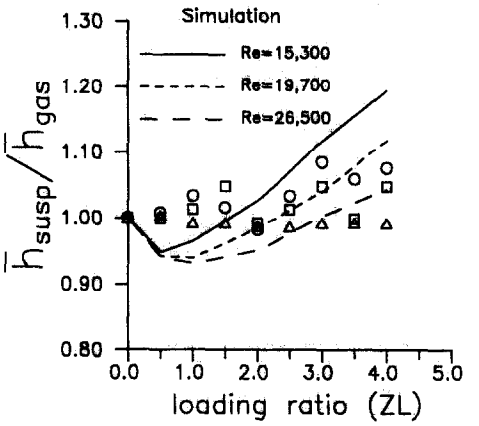

Fig. 6. Ratio of heat transfer coefficients vs loading ratio, for various Re (Farbar and Depew experiment, $d_p = 200 \times 10^{-6}$ m, ○ Re = 15 300, □ Re = 19 700, △ Re = 26 500).

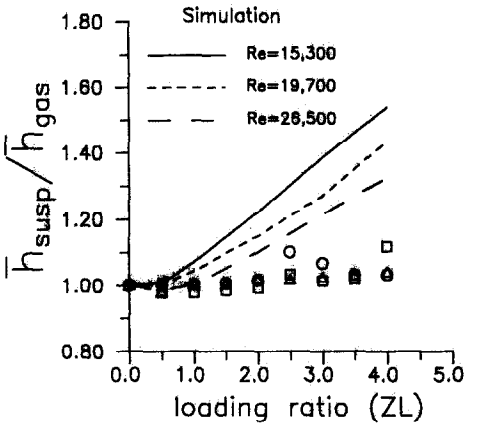

Fig. 7. Ratio of heat transfer coefficients vs loading ratio, for various Re (Farbar and Depew experiment, $d_p = 140 \times 10^{-6}$ m, ○ Re = 15 300, □ Re = 19 700, △ Re = 26 500).

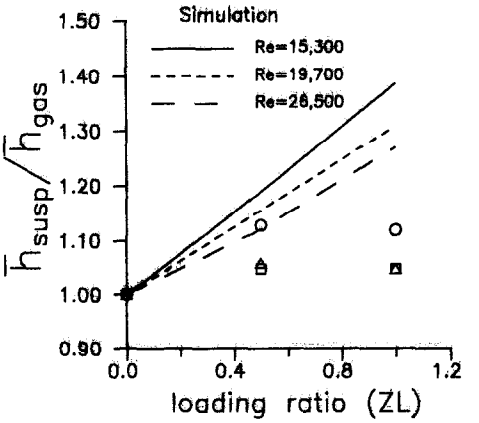

Fig. 8. Ratio of heat transfer coefficients vs loading ratio, for various Re (Farbar and Depew experiment, $d_p = 70 \times 10^{-6}$ m, ○ Re = 15 300, □ Re = 19 700, △ Re = 26 500).

Figures 6–8 show the comparison between the numerical predictions and the experimental data of Farbar and Depew [4]. In the figures $\bar{h}_{gas}$ represents

the clean gas average heat transfer coefficient for the corresponding Reynolds number.

It is found that, when the loading ratio is around 1, the particles promote a decrease in $\bar{h}_{susp}$. An explanation of this behavior is that the particles decrease the turbulence level of the gas phase (as was observed in the prediction of Tsuji *et al.* experiment). With this ZL value (around 1), the suspension heat capacity has a neglegible effect on the average heat transfer coefficient.

Figure 6 shows that, when the particles are relatively large ($d_p = 200$ μm), the effect on $\bar{h}_{susp}$ is small if ZL increases beyond 1. On the other hand Figs. 7 and 8 indicate that, if the particles are relatively small ($d_p < 140$ μm), the average heat transfer coefficient increases considerably when $ZL > 2$. Farbar and Depew reported that, when the particle diameter was greater than 70 μm, the heat transfer to the suspension decreased.

The size of the particles plays an important role in the behavior of $\bar{h}_{susp}$, i.e. smaller particles (small thermal characteristic time) convey more heat along the pipe so that the suspension heat capacity effect is greater. Farbar and Morley [7] and Chu and Depew [16] reported that small particles contribute more than larger ones to the heat transfer rate.

Figures 7 and 8 indicate that the experimental data are overpredicted, especially when $ZL > 1$, probably because the experimental value of $\bar{h}_{susp}$ was obtained by assuming that the particles had the same temperature as the fluid both at the inlet and at the outlet of the test section.

The heat transfer coefficient depends on the suspension Reynolds number because it is a measure of the particles' residence time in the heated duct, and as was mentioned by Farbar and Morley [7], the smaller the Reynolds number, the longer the time that the particles have to absorb heat from the fluid. This behavior was verified in the simulation and is indicated in Figs. 6 and 7. Figure 6 shows that if $Re_D = 15\,300$ and $ZL < 1$, the effect of the suspension heat capacity is more important, i.e. $\bar{h}_{susp}$ does not decrease markedly due to the turbulence modulation. On the other hand, in Fig. 6 it is observed that when $Re_D = 26500$ the effect of increased heat capacity is not significant (small particle residence time), so that the turbulence modulation promotes a decrease in $\bar{h}_{susp}$. Figure 7 shows very clearly the effect of the suspension Reynolds number on $\bar{h}_{susp}$. In this figure it can be observed that, for a particle loading ratio less than 1 and $Re_D = 26500$ (small particle residence time), $\bar{h}_{susp}$ decreases due to the turbulence modulation and the small effect of the suspension heat capacity. But for the same particle loading ratio and $Re_D = 15300$ (large residence time), $\bar{h}_{susp}$ does not decrease.

Figures 6–8 indicate that the average heat transfer coefficient increases faster when the Reynolds number is small ($Re_D = 15300$). This corresponds with Jepson *et al.* [11], who reported that, for high Reynolds numbers (high turbulence level), the viscous sublayer is thin enough that the injection of solid particles beyond $ZL = 1$ does not produce an additional increase in either the turbulence of the gas phase or the average heat transfer coefficient.

8. CONCLUDING REMARKS

Numerical predictions of an isothermal particulate pipe flow were performed, in order to analyse the behavior of the average heat transfer coefficient in nonisothermal turbulent pipe flows loaded with solid particles. It was found that the particles concentrate around the center of the pipe and interact significantly with the turbulence of the gas phase, causing a reduction in turbulent fluctuations. The average heat transfer coefficient, calculated using a logarithmic mean temperature difference, as well as the heat conveyed by the suspension along the pipe, acquire minimum values in the range $0 < ZL < 1$.

The numerical computations are in satisfactory agreement with experimental data and it is found that large particles (200 μm), do not increase heat transfer from the isothermal wall, whereas small particles (70 and 140 μm) cause a linear increase in the heat transfer coefficient.

From this numerical simulation, the following may be concluded:

The average heat transfer coefficient $\bar{h}_{susp}$ increases when the particle loading ratio is greater than 1.

$\bar{h}_{susp}$ is a function of the particle size, particle loading ratio and suspension Reynolds number.

When $ZL < 1$ there are two effects which combine to modify $\bar{h}_{susp}$.

The turbulence decrease effect is large and the suspension heat capacity effect is small. Hence a net reduction in $\bar{h}_{susp}$ is produced.

For small particles ($d_p < 140$ μm), the suspension heat capacity effect is more significant than the effect produced by the turbulence modulation. Hence a net increase in $\bar{h}_{susp}$ is produced.

For high suspension Reynolds numbers, the effect of the particles on $\bar{h}_{susp}$ is relatively low.

Acknowledgement—The first author wishes to thank Miss Kimberly Anderson from the University of California at Berkeley, for her assistance in the preparation of the manuscript.

REFERENCES

1. D. Stockburger (Heat Transmission between a Tube Wall and a Turbulently Flowing Gas–Solids Mixture (Flying Dust)), *Der Warmeaustausch zwischen einer Rohrwand und einem turbulent stromenden Gas–Feststoff–Gemisch*. VDI, Düsseldorf, (Forschungsheft 518) (1966).
2. R. Pfeffer, S. Rosseti and S. Lieblein, Analysis and correlation of heat-transfer coefficient and friction factor data for dilute gas–solid suspensions, NASA Technical Note D–3603, Washington, DC September (1966).
3. C. A. Depew and T. J. Kramer, Heat transfer to flowing

gas–solids mixtures, *Adv. Heat Transfer* **9,** 113–180 (1973).
4. L. Farbar and C. A. Depew, Heat transfer effects to gas–solids mixtures using solid spherical particles of uniform size, *I E C Fundam.* **2,** (2), 130–135 (1963).
5. K. S. Han, H. J. Sung and M. K. Chung, Analysis of heat transfer in a pipe carrying two-phase gas-particle suspension, *Int. J. Heat Mass Transfer* **34** (4), 69–78 (1991).
6. C. L. Tien, Heat transfer by a turbulently flowing fluid–solids mixture in a pipe, *Trans. ASME Ser. C. J. Heat Transfer* **83,** 183–188 (1961).
7. L. Farbar and M. J. Morley, Heat transfer to flowing gas–solids mixtures in a circular tube, *Indust. Engng Chem.* **49** (7), 1143–1150 (1957).
8. V. S. Nosov and N. I. Syromyatnikov, Laws of heat loss for finely dispersed flows, *Sov. Phys. Dok.* **10** (7), 672–674 (1966).
9. G. T. Wilkinson and J. R. Norman, Heat transfer to a suspension of solids in a gas, *Trans. Inst. Chem. Engrs* **45,** 314–318 (1967).
10. A. A. Shrayber, Turbulent heat transfer in pipe flows of gas-conveyed solids, *Heat Transfer Sov. Res.* **8** (3), 60–67 (1976).
11. G. Jepson, A. Poll, W. Smith, Heat transfer from gas to wall in a gas–solids transport line, *Trans. Inst. Chem. Engrs* **41,** 207–211 (1963).
12. R. G. Boothroyd and H. Haque, Fully developed heat transfer to a gaseous suspension of particles flowing turbulently in ducts of different size, *J. Mech. Engng Sci.* **12,** (3), 191–200 (1970).
13. R. G. Boothroyd and H. Haque, Experimental investigation of heat transfer in the entrance region of a heated duct conveying fine particles, *Trans. Inst. Chem. Engrs,* **48,** 109–120 (1970).
14. R. S. Kane, R. Pfeffer, Heat transfer in gas–solids drag—reducing flow, *Trans. ASME J. of Heat Transfer* **107,** 570–574 (1985).
15. E. E. Michaelides, Heat transfer in particulate flows, *Int. J. Heat Mass Transfer* **29,** (2), 265–273 (1986).
16. N. C. Chu and C. A. Depew, Heat transfer to gas–solids suspension flows in vertical circular tubes, *Proc.* 1972 *Heat Transfer and Fluid Mechanics Institute,* pp. 371–385 (1972).
17. Y. Tsuji, Y. Morikawa and H. Shiomi, LDV measurements of an air–solid two-phase flow in a vertical pipe, *J. Fluid Mech.* **139,** 417–434 (1984).
18. D. Milojevic, Lagrangian stochastic-deterministic model (LSD) for the prediction of turbulent fluid–particle flows, *Second Workshop on Two-phase Flow Predictions,* Lehrstühl für Strömungstechnik, Universtät Erlangen-Nürnberg, Germany (1985).
19. B. E. Launder and D. B. Spalding, The numerical computation of turbulent flows, *Comput. Meth. Appl. Mech. Engng* **3,** 269–289 (1974).
20. G. B. Wallis, *One Dimensional Two-Phase Flow.* McGraw-Hill, New York (1969).
21. C. T. Crowe, M. P. Sharma and D. E. Stock, The particle-source-in cell (PSI-CELL) model for gas–droplet flow, *Trans. ASME J. of Fluids Engng* (1977).
22. Martin R. Maxey and James J. Riley, Equation of motion for a small rigid sphere in a nonuniform flow, *Phys. Fluids* **26** (4), 883–889 (1983).
23. J-S. Shuen, A. S. P. Solomon, Q. F. Zhang and G. M. Faeth, Structure of particle-laden jets: measurements and predictions, *AIAA J.* **23,** (3).
24. R. Weber, F. Boysan, W. H. Ayers and J. Swithenbank, Simulation of dispersion of heavy particles in confined turbulent flows, *AIChe J.* **30,** (3), 490–492 (1984).
25. R. Clift, J. R. Grace and M. E. Weber, *Bubbles, Drops and Particles.* Academic Press, New York (1978).
26. S. Corrsin, Estimates of the relations between Eulerian and Lagrangian scales in large Reynolds number turbulence, *J. Atmos. Sci.* **20,** 115–119 (1963).
27. B. E. Launder, Heat and mass transport. In *Turbulence* (Edited by P. Bradshaw). Springer, Berlin (1978).
28. S. V. Patankar and D. B. Spalding, *Heat and Mass Transfer in Boundary Layers.* Intertext, London, (1970).
29. S. V. Patankar, Numerical heat transfer and fluid flow. In *Computational methods in Mechanics and Thermal Sciences.* Mc-Graw Hill, New York (1980).
30. S. Wittig, W. Rodi, K. H. Sill, S. Eriksen, K. Rtd, G. Scheuerer and A. Schulz, Gasturbinen-Schaufelkühlung-programmbeschreibung ALFA, Institut für Thermische Strömungsmaschinen, Universität Karlsruhe, Vorhaben No. 241 (1983).
31. D. B. Spalding, *GENMIX—a General Computer Program for Two-Dimensional Parabolic Phenomena.* Pergamon Press, Oxford (1977).
32. T. J. Kramer and C. A. Depew, Analysis of mean flow characteristics of gas–solids suspensions, *Trans. ASME, J. Basic Engng* **94,** (4), 731–738 (1972).
33. F. P. Incropera and D. P. Dewitt, *Fundamentals of heat and Mass Transfer* (2nd Edn). Wiley, New York (1985).